HHS Public Access

Author manuscript

Photochem Photobiol. Author manuscript; available in PMC 2018 January 30.

Published in final edited form as:

Photochem Photobiol. 2017 January ; 93(1): 331–342. doi:10.1111/php.12697.

Kinetic Isotope Effects and Hydrogen/Deuterium Exchange Reveal Large Conformational Changes During the Catalysis of the *Clostridium acetobutylicum* Spore Photoproduct Lyase†

Linlin Yang[1,¶], **Jagat Adhikari**[2,¶], **Michael L. Gross**[2], and **Lei Li**[1,3]

[1]Department of Chemistry and Chemical Biology, Indiana University-Purdue University Indianapolis (IUPUI), 402 North Blackford Street, Indianapolis, Indiana, 46202, USA

[2]Department of Chemistry, Washington University in St. Louis, One Brookings Dr., St. Louis, MO 63130, USA

[3]Department of Biochemistry and Molecular Biology & Department of Dermatology, Indiana University School of Medicine, Indianapolis, Indiana 46202, USA

Abstract

Spore photoproduct lyase (SPL) catalyzes the direct reversal of a thymine dimer 5-thyminyl-5,6-dihydrothymine (i.e., the spore photoproduct (SP)) to two thymine residues in germinating endospores. Previous studies suggest that SPL from the bacterium *Bacillus subtilis* (*Bs*) harbors an unprecedented radical transfer pathway starting with cysteine 141 proceeding through tyrosine 99. However, in SPL from the bacterium *C. acetobutylicum* (*Ca*), the cysteine (at position 74) and tyrosine are located on the opposite sides of a substrate binding pocket that has to collapse to bring the two residues into proximity, enabling the C→Y radical passage as implied in $SPL_{(Bs)}$. To test this hypothesis, we adopted hydrogen/deuterium exchange mass spectrometry (HDX MS) to show that $C74_{(Ca)}$ is located at a highly flexible region. The repair of dinucleotide SP TpT by $SPL_{(Ca)}$ is 8–10-fold slower than that by $SPL_{(Bs)}$; the process also generates a large portion of the aborted product $TpTSO_2^-$. $SPL_{(Ca)}$ exhibits apparent ($^D V$) kinetic isotope effects (KIEs) of ~ 6 and abnormally large competitive ($^D V/K$) KIEs (~ 20), both of which are much larger than the KIEs observed in $SPL_{(Bs)}$. All these observations indicate that $SPL_{(Ca)}$ possesses a flexible active site and readily undergoes conformational changes during catalysis.

Graphical abstract

†This article is part of the Special Issue highlighting Dr. Aziz Sancar's outstanding contributions to various aspects of the repair of DNA photodamage in honor of his recent Nobel Prize in Chemistry.

Corresponding authors': mgross@wustl.edu (Michael L. Gross), lilei@iupui.edu (Lei Li).
¶These authors contributed equally to the work.

SUPPORTING INFORMATION

Additional Supporting Information is available in the online version of this article:

Figure S1. SDS-PAGE showing the purified SPL(Bs) and SPL(Ca) proteins used in this study.

Figure S2. (A) Electrospray mass spectrum of SPL(Ca) protein acquired under denaturing condition, and (B) molecular weight determined (41119.0 Da) from the deconvolved mass spectrum. The SPL(Ca) protein contained the expression tag with the initiator methionine residue cleaved off.

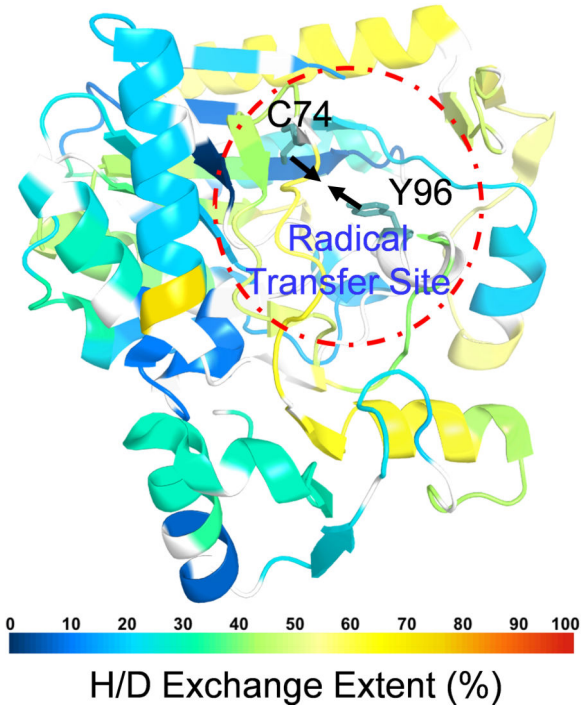

Spore photoproduct lyase (SPL) repairs 5-thyminyl-5,6-dihydrothymine (i.e., the spore photoproduct (SP)) using a radical transfer pathway that includes at least a cysteine and a tyrosine in germinating endospores. In SPL from the bacterium *C. acetobutylicum*, these two residues (cysteine 74 and tyrosine 96) are located on the opposite sides of a substrate binding pocket that has to collapse to bring the two residues into proximity, enabling the C→Y radical passage. Here, we describe the experimental evidence obtained via hydrogen/deuterium exchange mass spectrometry (HDX MS) and enzyme kinetics studies to support this hypothesis.

INTRODUCTION

5-Thyminyl-5,6-dihydrothymine is the dominant DNA photolesion found in UV or solar irradiated bacterial endospores. It accounts for > 95% of DNA photolesions in UVC irradiated spores, making spore DNA the only known system in nature where DNA photoreaction produces one single dominant photoproduct. Therefore, this thymine dimer is commonly referred to as the spore photoproduct (SP) (1–4). SPs accumulate in spores that have no detectable metabolism, and as many as 28% of total Ts in spores can be converted to SPs. Thus, during the first few hours when spores start germination and outgrowth, these SPs must be repaired mainly via a direct reversal mechanism mediated by the spore-unique spore photoproduct lyase (SPL) (4, 5). The proper function of SPL is important for spore survival from UV irradiation as unpaired SPs prove lethal to the germinated bacteria (6, 7).

SPL belongs to the so-called radical SAM (*S*-adenosylmethionine) enzyme superfamily (5, 8–11). The superfamily is defined by the characteristic tri-cysteinyl motif: CX_3CX_2C that binds to a [4Fe-4S] cluster. Once reduced to the 1+ oxidation state, the cluster can then donate an electron to the sulfonium ion of SAM to cleave it reductively to produce a 5'-

deoxyadenosyl radical (5'-dA•) and a methionine. The 5'-dA• abstracts the H_{6pro}*R* atom to initiate the SP repair process (12, 13), and the resulting thymine allylic radical receives an H-atom from a conserved cysteine, C141 in *B. subtilis* (*Bs*) SPL, yielding the repaired thymine residues (Figure 1) (14, 15). This process leaves a thiol radical on the enzyme, which is hypothesized to abstract an H-atom from the neighboring $Y99_{(Bs)}$. The $Y99_{(Bs)}$ radical then oxidizes the 5'-dA under the assistance of Y97, yielding the 5'-dA• before regenerating the SAM molecule (16). This mechanism indicates that SPL harbors an unprecedented radical transfer pathway involving one cysteine and two tyrosine residues as essential elements.

The existence of the radical transfer pathway is supported by the SPL structure from the bacterium *Geobacillus thermodenitrificans (Gt)* (17), which is a thermophilic *Bacillus*. $SPL_{(Gt)}$ shares ~ 77% sequence identity with $SPL_{(Bs)}$, but exhibits a −1 sequence shift for the conserved amino acids. The crystal also contained an uncleaved SAM molecule and a dinucleoside SP (Figure 2). The distance between the methylene carbon of SP and the conserved cysteine ($C140_{(Gt)}$) is 4.5 Å, which may be even shorter after the SP fragmentation to yield a thymine methyl radical. This conserved cysteine, thus, is well-positioned to be the H-donor as predicted by enzymology studies. The $Y98_{(Gt)}$ residue, located between $C140_{(Gt)}$ and SAM, is 5.1 Å from $C140_{(Gt)}$ and 3.6 Å from the C5' of SAM, indicating that it serves as a key intermediate in the radical-transfer pathway. The $Y96_{(Gt)}$ is located at the other side of SAM interacting with the adenosyl ring, potentially justifying its role as the radical delocalizer to facilitate the regeneration of 5'-dA• before the regeneration of SAM.

Both *Bacillus* and *Clostridium* strains form endospores; SPLs from these strains very likely share the same mechanism. As indicated by the $SPL_{(Gt)}$ structure, a radical transfer between $C140_{(Gt)}$ and $Y98_{(Gt)}$ is likely. However, unlike the two tyrosine residues conserved at similar positions in all SPL enzymes, the conserved cysteine is located at a different region in *Clostridium* SPLs; that is, at position 74 before the radical SAM domain in *Clostridium acetobutylicum* (*Ca*) SPL (Figure 3), which corresponds to S77 in $SPL_{(Bs)}$. Given the 42% sequence identities between $SPL_{(Bs)}$ and $SPL_{(Ca)}$, these proteins likely possess similar 3D structures. In $SPL_{(Gt)}$, $S76_{(Gt)}$ (S77 in $SPL_{(Bs)}$) resides on the tip of a loop and is only 4.2 Å away from the SP methylene carbon but 7.5 Å away from the conserved $Y98_{(Gt)}$ (Figure 2). If C74 is indeed the H-donor, as suggested by a recent mutational study (18), the resulting $C74_{(Ca)}$-S• radical would have to move a relatively long distance before it can oxidize $Y96_{(Ca)}$ should the CY-based radical transfer pathway exist in $SPL_{(Ca)}$.

Damaged nucleotides are usually flipped into enzyme-binding pockets for repair (19–24); the repaired nucleotides are flipped back to restore the stacked DNA conformation before DNA is released. SPL likely adopts a similar strategy; its conformation must change during the SP flip-in and TpT flip-out processes. In Figure 2, the dinucleoside SP is found between $S76_{(Gt)}$ and $Y98_{(Gt)}$ (17); such a structure likely reflects the SP flip-in conformation. After TpT is flipped out, $SPL_{(Ca)}$ may collapse the active site to move $C74_{(Ca)}$ and $Y96_{(Ca)}$ into proximity, allowing the radical transfer to occur. If such a hypothesis is true, then $SPL_{(Ca)}$ is expected to have a flexible substrate binding pocket, enabling the large protein conformational change.

Using hydrogen/deuterium exchange coupled to mass spectrometry (HDX-MS), we obtained evidence to support this hypothesis and prove that $C74_{(Ca)}$ is located at a highly flexible region. Examination of the $SPL_{(Ca)}$ activity using dinucleotide SP TpT, which exhibits a weak enzyme binding affinity as the enzyme substrate, revealed a 10-fold slower repair activity mediated by $SPL_{(Ca)}$ than that by $SPL_{(Bs)}$. A significant amount of runaway product TpT-SO_2^- was also found in the $SPL_{(Ca)}$ reaction. These observations, coupled with the measurement of kinetic isotope effects, support our assumption that large protein conformational changes, enabled by the flexible enzyme active site, occur during the $SPL_{(Ca)}$ catalysis.

METHODS

Materials

DNA-modifying enzymes were purchased from Fermentas Life Sciences (Glen Burnie, MD). Oligonucleotide primers used for gene cloning were synthesized by Integrated DNA Technologies (Coralville, IA). *E. coli* BL21 (DE3), and the expression vector pET-28a was purchased from Novagen (Madison, WI). *Clostridium acetobutylicum* genomic DNA was purchased from the ATCC (ATCC 824). 5 Prime Perfectpro* Nickel nitrilotriacetic acid (Ni-NTA) resin was purchased from Fisher Scientific. Deuterium oxide was purchased from Cambridge Isotope Laboratories Inc. (Andover, MA). All chemicals, proteases, and solvents were purchased from Sigma-Aldrich (St. Louis, MO) unless otherwise stated.

Preparation of SP TpT substrates

The dinucleotide SP TpT was synthesized as previously described (25). The d_3- and d_4-SP were photochemically synthesized using respective dinucleotide d_3-TpT containing a $-CD_3$ group at the 3′-thymine and d_4-TpT with all four non-exchangeable hydrogen atoms at the 5′-thymine replaced by deuterium in dry-film reactions (25).

Construction of $SPL_{(Ca)}$ expression vector

The *splB* gene was cloned from the *C. acetobutylicum* genomic DNA using the synthetic oligonucleotide primers 5′-GAGCATATGGAAAATATGTTTAG AAGAGTTATATTTG-3′ (containing a NdeI site) and 3′-GAGGAATTCTTAAATTATATACTTAAT TGTTGCCTTG-5′ (containing an EcoRI site) and amplified by standard PCR techniques. The resulting PCR product was digested by EcoRI/NdeI and ligated into the same sites in pET-28a. The construct was transformed into *E. coli 10 G* chemically competent cells purchased from Lucigen Corporation (Middleton, WI) for isolation and amplification of the *splB* gene-containing plasmid DNA. The resulting vector was named SPL(Ca)-pET28 and co-transformed with a pDB 1282 vector into *E. coli* BL21(DE3) obtained from Stratagene (La Jolla, CA) for protein overexpression. The pDB 1282 vector confers ampicillin resistance and harbors an *E. coli* operon that is involved in the biosynthesis of FeS clusters; thus, it may facilitate incorporation of the FeS clusters into the apoprotein of SPL (26, 27).

Expression of $SPL_{(Ca)}$

A single colony of transformed cells was used to inoculate 5 mL of LB medium containing the appropriate antibiotics to maintain selection for the plasmid. The cultures were grown to

saturation at 37 °C with vigorous shaking and then used to inoculate 1 L of antibiotics containing LB medium. Once the cells reached early log phase (OD_{600} ≈ 0.8), the temperature was reduced to 16 °C, and the gene expression induced by addition of isopropyl β-D-thiogalactopyranoside (IPTG) to a final concentration of 0.3 mM. The expression was allowed to proceed for 16 h, and the cells harvested by centrifugation.

Purification of $SPL_{(Bs)}$ and $SPL_{(Ca)}$

The $SPL_{(Bs)}$ was cloned, expressed, and purified as previously described (13, 14). The $SPL_{(Ca)}$ was purified under similar protocols used for $SPL_{(Bs)}$.

Iron and sulfide assays

The iron and sulfur contents in $SPL_{(Ca)}$ were measured via assays described previously (13, 14).

SPL activity assay

SPL activity was analyzed as previously described (16). Typically, a reaction mixture contained 1.2 nmol SPL (either $SPL_{(Bs)}$ or $SPL_{(Ca)}$), 36 nmol SP TpT substrate, and 6 nmol SAM in 400 μL buffer containing 25 mM Tris-HCl, 250 mM NaCl, and 10% glycerol at pH 7.0. These components were incubated for 30 min, and then 400 nmole sodium dithionite was added to reduce the [4Fe-4S] cluster and initiate the reaction. The reaction was carried out under anaerobic conditions at ambient temperature for various periods of time. At each time point, 40 μL of the solution was aliquoted and quenched by acid (13, 14, 16). After removing protein via extraction with phenol/chloroform, the supernatant fluids were loaded onto an HPLC and analyzed using procedures described below.

Deuterium kinetic isotope effects (KIEs)

The apparent (^{D}V) KIEs for $SPL_{(Ca)}$ were measured by direct comparison of the initial rates with SP TpT and d_4-SP TpT as the enzyme substrates, respectively. The competitive ($^{D}(V/K)$) KIE was determined using the internal competition approach with an equimolar mixture of SP TpT and d_4-SP TpT at 1 mM total concentration. The experimental details for the KIE determination can be found in our previous publications (13, 14, 28).

HPLC assay

HPLC was performed with detection at 260 nm using a Shimadzu LC-20AB high-pressure gradient solvent delivery unit coupled with a SPD-20A UV-Vis detector and a CTO-10AS VP Column Oven. A Waters XBridge™ OST reversed-phase C18 column (2.5 μm, 4.6 × 50 mm) was used for all separation work. Analysis of dinucleotide SP TpT repair was conducted by using our previously described HPLC procedure where 50 mM triethylammonium acetate at pH 6.5 was used as Mobile Phase A, and the compounds were eluted with an ascending gradient (0 – 25%) of Mobile Phase B which was composed of 50% Mobile Phase A and 50% acetonitrile at a flow rate of 1 mL/min (11, 13, 14).

LC-MRM-MS analysis

SP repair by SPL was analyzed via an Agilent 1200-6410 LC-MS triple quadrupole mass spectrometer operating in the multiple reaction monitoring (MRM) mode. The HPLC experiments used a ZORBAX Eclipse plus C18 column 4.6 × 50 mm (3.5 μm in particle size, Agilent Technologies, Santa Clara, CA) at ambient temperature with a flow rate of 500 μL/min. A solution of 5 mM ammonium acetate in water (Mobile Phase A) and a solution of 5 mM ammonium acetate in 1 : 1 methanol/acetonitrile (Mobile Phase B) were used for the analysis of SP TpT and TpT; the gradient started with 5% Mobile Phase B for 1 min followed by a gradient of 1% per min for 25 min. Sufficiently intense mass spectrometric signals were obtained for SP TpT and TpT; however, the $TpTSO_2^-$ signal was weak possibly because non-volatile residual cations quenched the signal. To ensure the accurate quantification of the $TpTSO_2^-$ signal, a SeQuant®ZIC®HILIC column (3 μm, 100 Å, PEEK 50 × 2.1 mm, EMD Millipore Corporation) was chosen, and the analysis conducted at ambient temperature at a chromatographic flow rate of 250 μL/min. Acetonitrile was used as the Mobile Phase A, and a solution of 5 mM ammonium acetate in water was used as the Mobile Phase B. The analysis started with 90% Mobile Phase A for 1 min followed by 2.5% per min increase of Mobile Phase B for 10 min. The HILIC column enabled better removal of the hard cations, resulting in more intense mass spectrometric signals to enable reliable $TpTSO_2^-$ quantifications.

The eluted compounds were introduced into an Agilent triple quadrupole mass spectrometer. The temperature for the sheath gas flow was maintained at 350 °C, the gas flow rate was 11 L/min, and the capillary voltage was 4 kV. Precursor ions of SP TpT and TpT (*m/z* 545.2), d_3-TpT (*m/z* 548.2) as well as d_4-SP TpT (*m/z* 549.2) were chosen. The voltage for fragmentation was optimized to 225 V for SP TpT as well as d_4-SP TpT and 130 V for TpT as well as d_3-TpT. Under such conditions, the fragments of *m/z* of 251.1 (34 V) and 195.0 (34 V) for SP TpT, *m/z* of 255.1 (34 V) and 195.0 (34 V) for d_4-SP TpT, *m/z* of 125.0 (34 V) for TpT, and *m/z* of 128.0 (34 V) for d_3-TpT were monitored in the negative-ion mode. The precursor ions of $TpTSO_2^-$ (*m/z* 609.1) as well as d_3-$TpTSO_2^-$ (*m/z* 612.1) were fragmented at a voltage of 130 V, and the fragments of *m/z* 125.0 (45 V) for TpT and *m/z* 128.0 (45 V) for d_3-$TpTSO_2^-$ in the negative-ion mode. The collision energy for each fragment was optimized (as listed in the parenthesis next to the fragment above). Linear responses between the intensity of mass spectrometric signals and the amount of the analytes were observed, demonstrating the feasibility of using this LC-MRM-MS/MS assay for quantitative analysis. Therefore, for the TpT and $TpTSO_2^-$ generated in the SPL reaction, their amounts were readily quantified by calculating from the peak area found in the selected-ion chromatograms for the analytes.

HDX-MS analysis of SPL

Continuous HDX labeling of SPL protein samples was performed as previously described (29). Briefly, stock solutions of 20 μM for both $SPL_{(Bs)}$ and $SPL_{(Ca)}$ proteins were prepared in 25 mM Tris buffer containing 250 mM NaCl and 10% glycerol at pH 7.0. At the start of each experiment, the H_2O and D_2O Tris buffers were degassed with N_2 for 5–10 min. Continuous labeling with deuterium was initiated by diluting 2 μL of the stock solution into 20 μL of 25 mM Tris-base containing 250 mM of NaCl in D_2O buffer. HDX control samples

(undeuterated) were prepared in the same way with an H_2O buffer. Quenching was performed under reducing conditions with ice-cold 3 M Urea in 1% TFA solution. HDX reactions were conducted at 25 °C, and the extent of HDX was measured at 0, 10, 30, 60, 120, 900 and 3600 s, and the reactions were stopped by adding 30 μL of quench buffer. Duplicate measurements were carried out for each time point. The acquired spectra were searched by using HDX workbench software (30). The percentage of deuterium uptake (D %) was mathematically adjusted because the exchange buffer contained 90% deuterium.

RESULTS

Protein expression and purification

We cloned the *splB* gene from *Clostridium acetobutylicum* into the pET 28a vector that introduced a hexahistidine tag to facilitate protein purification. Ni-NTA chromatography afforded SPL as a dark-brown solution when purified under a strictly inert atmosphere. The purity of the protein was checked by SDS-PAGE to be > 95%, and the purified SPL exhibited a single band at ~ 40 kDa (Supporting Information, Figure S1). A typical yield for such a SPL purification process is ~30 mg protein per liter of LB media. The as-isolated SPL protein exhibited a UV absorption at 408 nm (Figure 4, ε = ~ 12,000 M^{-1} cm^{-1}), which is characteristic of a $[4Fe\text{-}4S]^{2+}$ cluster in the 2+ oxidation state (31). The presence of the [4Fe-4S] cluster in SPL was further confirmed by an iron and sulfur content analysis. The as-isolated SPL was found to contain 3.5 ± 0.3 iron and 3.3 ± 0.4 sulfur atoms per protein, further supporting this conclusion.

Dinucleotide SP TpT repair

Our previous studies show that $SPL_{(Bs)}$ repairs SP TpT with a reasonably high activity, exhibiting a turnover number of up to 0.40 min^{-1} (13, 14). Moreover, a careful analysis of the reaction products reveals a small amount of TpT-SO_2^-, accounting for ~ 5% of the overall SP TpT repaired (Figure 5). As shown in the previous studies (14, 32), TpT-SO_2^- is the dominant SP TpT repair product by $SPL_{(Bs)}$ C141A mutant in which the intrinsic H-atom donor C141 no longer exists, and the vast majority of the thymine allylic radical intermediate is quenched by the externally added dithionite anion likely after its release from the protein. The formation of TpT-SO_2^- in our current study indicates that a small portion of this intermediate escapes from the wildtype $SPL_{(Bs)}$ active site.

Surprisingly, $SPL_{(Ca)}$ exhibited a much lower enzyme activity compared with $SPL_{(Bs)}$, generating TpT at a rate of 0.04 ± 0.01 min^{-1} (Figure 6), which is 8–10 fold slower than the TpT formation observed in the $SPL_{(Bs)}$ reaction. Interestingly, the reaction generated a significant amount of TpT-SO_2^-; the formation rate of which was determined to be 0.010 ± 0.002 min^{-1}, indicating that 20–25% of the SP TpT molecules repaired were prematurely released after the generation of the thymine allylic radical intermediate that was then quenched by the external dithionite anion (14, 32, 33). The enhanced formation of the runaway product TpT-SO_2^- suggests that $SPL_{(Ca)}$ possesses a much more flexible active site than $SPL_{(Bs)}$.

Apparent (^{D}V) kinetics isotope effect (KIE) determination

To confirm further this result, we compared the initial rates of the $SPL_{(Ca)}$ reaction using SP TpT and d_4-SP TpT as the substrates, respectively. The d_4-SP TpT contains a -CD_3 group and a deuterium at the H_{6proR} position of the 5'-nucleoside (25). As established in our previous studies (13), the 5'-dA radical generated from the SAM reductive cleavage step abstracts the H_{6proR} atom to initiate the SP repair process (Figure 1). This step is slower when the deuterium in d_4-SP TpT is abstracted, slowing the overall repair process and resulting in the $^{D}V_{max}$ KIE in the steady state enzyme kinetics. Because $SPL_{(Ca)}$ exhibits a linear behavior only within the first turnover and, thus, possesses a very short "steady state", we term the derived $^{D}V_{max}$ KIEs as apparent (^{D}V) KIEs, similar to those used in our previous SPL studies (13, 14).

Our previous studies showed that the abstracted deuterium from d_4-SP by 5'-dA• is not returned to the repaired TpT (13), and only three deuterium atoms are retained in the TpT product. Therefore, the d_4-SP TpT repair results in d_3-TpT and d_3-$TpTSO_2^-$. In our hands, $SPL_{(Ca)}$ produced d_3-TpT at 0.007 ± 0.001 min^{-1} and d_3-$TpTSO_2^-$ at 0.0017 ± 0.0002. Both products were formed at slower rates than those with unlabeled SP. Comparing these numbers leads to the apparent (^{D}V) KIE of 6.1 ± 0.7 for TpT and 5.8 ± 1.0 for $TpTSO_2^-$.

Competitive ($^{D}V/K$) KIE determination

Besides the (^{D}V) KIEs, we also measured the ($^{D}V/K$) KIE for the $SPL_{(Ca)}$ reaction by using the 1:1 mixture of SP TpT and d_4-SP TpT (13, 14). The SP repair subsequently generates a mixture of TpT and d_3-TpT, which co-elute by HPLC; the relative amount of these two species can be determined by an MS/MS analysis in the MRM mode. As shown in Figure 7A, one of the major product ions generated from the TpT fragmentation is the release of the 5'-thymine anion; the product ion resulting from d_3-TpT carries three deuterium atoms and exhibits a + 3 Da shift relative to its unlabeled counterpart. Therefore, it can be used as the marker to distinguish the fragment signals of TpT and d_3-TpT, enabling us to determine accurately the ratio between these two species. $TpTSO_2^-$, following selection of its precursor ion by MS1, also generates the same 5'-thymine daughter ion in MS2 (Figure 7B), allowing the d_0/d_3-$TpTSO_2^-$ ratio to be quantified as well.

The competitive KIEs were measured at relatively low extents of reaction of between 1% and 15%. Under these conditions, the isotopic composition of the starting SP varies nearly linearly with the extent of reaction. Therefore, we could calculate the competitive ($^{D}V/K$) KIE by linear extrapolation of the kinetic isotope effects measured at various reaction extents to zero extent reaction (Figure 8), resulting in 17.0 ± 2.0 for the TpT formation and 21.0 ± 2.0 for the $TpTSO_2^-$ formation. Both numbers are much larger than the competitive KIEs determined from our previous studies with both wildtype and mutant $SPL_{(Bs)}$ enzymes (13, 14, 16).

HDX-MS analysis of the $SPL_{(Bs)}$ and $SPL_{(Ca)}$ proteins

To gain further insight into the enzyme behavior, we looked at the levels of deuterium uptake for the $SPL_{(Bs)}$ and $SPL_{(Ca)}$ proteins by using HDX-MS. The average deuterium uptake percentage calculated for the duplicate analysis from seven time points for each of the

peptides produced upon pepsin digestion are depicted in the sequence coverage map for the $SPL_{(Bs)}$ (Figure 9) and $SPL_{(Ca)}$ (Figure 11), respectively. In Figures 9 and 11, the HDX kinetics for peptides from the same region with varying lengths and different charge states are also included.

Overall, the peptides neighboring the binding sites reveal higher deuterium uptake levels as shown in HDX kinetics map (Figures 9 and 11). According to the crystal structure of Benjdia et al. (17), S77 and C141 are both located on the tip of loops and should be flexible. The movement of these loops may place the residues at the "correct" distance to facilitate radical transfer. Therefore, we can assume that the enhanced flexibility of these loops will result in more H/D exchange. Such a hypothesis is supported by the HDX data. The peptides containing these two regions in $SPL_{(Bs)}$ (Figures 10B and 10F respectively) readily exchange deuterium, reaching ~60% saturation even within the first minute of exchange (Figures 9 and 10).

The HDX coverage map and the representative plots of $SPL_{(Ca)}$ reveal similar trends of deuterium uptake as was observed for $SPL_{(Bs)}$ for most part of the $SPL_{(Ca)}$ protein (Figures 11 and 12). As indicated by the $SPL_{(Gt)}$ structure where the S76 is on the tip of a loop (Figure 2), the $C74_{(Ca)}$ residue is projected to reside at the same region. However, we were unable to observe peptide 72–79 containing this residue in $SPL_{(Ca)}$ and are unable to report HDX kinetics for this region. We then measured the mass of the intact $SPL_{(Ca)}$ protein by ESI and under denaturing conditions and found its mass was −2 Da than expected, indicating a potential disulfide in this region (Supporting Information, Figure S2). We then attempted to reduce the disulfide bonds in the quench stage of HDX and before LC/MS analysis, but were not successful. We suggest that disulfide bond formation is likely the reason for missing peptides from this region. The result is the sequence coverage obtained is 95% for the $SPL_{(Ca)}$ protein (Figure 11), whereas 99% in the $SPL_{(Bs)}$ HDX studies.

Although the peptide containing the C74 residue is missing, the peptides representing regions prior and after this region give higher levels of deuterium uptake, suggesting that the intermediate region should also be flexible (Figures 12B, C and F respectively). The peptides from the C-terminus of the binding site in $SPL_{(Ca)}$, however, show greater protection as compared to the $SPL_{(Bs)}$ from the same region (Figures 12D and 10D respectively). More interestingly, the peptides (32–54) representing regions towards the N-terminus of the binding sites in $SPL_{(Ca)}$ show a higher deuterium uptake at ~60% (Figure 11 and 12 A) than the peptide regions in the same region in $SPL_{(Bs)}$ ~20% (Figure 9 and 10 A). This region is likely responsible for the greater flexibility in the binding pocket of $SPL_{(Ca)}$ as was implied by the enzymology studies. Overall, despite our inability to detect the C74-containing peptide, the HDX results corroborate the enzymology data with $SPL_{(Ca)}$.

DISCUSSION

Spore photoproduct lyase is the first enzyme, and the only one found to date, to utilize a novel radical-transfer pathway for catalysis in the large radical SAM superfamily, which may contain at least 48,000 enzymes as of 2014 (9) and ~110,000 enzymes according to the latest review (34). These enzymes can be found in almost all kingdoms of life and are

involved in catalysis of a wide range of vital processes including sulfuration, methylation, methylthiolation, hydroxylation, C-C bond formation or fragmentation, dehydrogenation, decarboxylation, metallocofactor maturation, and structural rearrangements (9). However, the vast majority of these enzymes have not been expressed *in vitro*, let alone undergone relatively detailed biological studies. The novel radical-transfer process exhibited by SPL represents a good model system, a better understanding of which can facilitate our understanding of other enzymes in this superfamily.

The radical-transfer pathway in $SPL_{(Bs)}$ starts at C141 after its H-donation to the thymine allylic radical (Figure 1) (14, 32). This cysteine is conserved in all SPL enzymes found in *Bacillus* strains, further supporting its role in enzyme catalysis. In contrast, in spore-forming *Clostridium* strains, the conserved cysteine is in a different region. In $SPL_{(Ca)}$, this cysteine is found at position 74. An enzymology study using a $C74A_{(Ca)}$ mutant found that the major SP repair product is $TpTSO_2^-$ (18), which is reminiscent of the SP repair catalyzed by the $C141A_{(Bs)}$ mutant. Although the crystal structure of $SPL_{(Gt)}$ implies that C74 is located at the enzyme active site, it also suggests that $SPL_{(Ca)}$ undergoes a relatively large conformational change to allow the cysteine and tyrosine residues, which are located on the opposite sides of the substrate binding pocket, to interact for radical passage and to maintain the integrity of the radical-transfer pathway shown in Figure 1.

The $SPL_{(Gt)}$ structure shows that both $C140_{(Gt)}$ and $S76_{(Gt)}$ are located at loop tips; therefore, both residues likely move with the protein during catalysis. Our HDX studies reveal that the amino acids on the loops containing C141 and S77 of $SPL_{(Bs)}$ undergo rapid HDX in aqueous solution. Although we could not detect the peptide fragment containing C74 of $SPL_{(Ca)}$, we observed that the regions immediately adjacent to the missing peptide undergo enhanced H/D exchange. Considering that the $SPL_{(Ca)}$ and $SPL_{(Bs)}$ exhibit ~ 42% identity in their primary sequence, implying they likely possess very similar 3D structures, we can reasonably conclude that the C74-containing loop in $SPL_{(Ca)}$ is highly mobile, supporting its role in participating in protein conformational changes during catalysis to maintain the integrity of the radical-transfer pathway.

Dinucleotide SP TpT is the smallest substrate for SPL with a presumably weak binding affinity. The K_m for SP TpT cannot be accurately determined in our hands owing to the weak substrate-enzyme interactions, although the K_m was estimated to be lower than 30 μM for $SPL_{(Bs)}$ (13). The enhanced active site mobility in $SPL_{(Ca)}$ implies that it may bind to SP TpT even more weakly and result in an even less stable Michaelis complex (SP-E), which subsequently lowers the fraction of the forward reaction from SP-E leading to a slower SP repair (Figure 13A). Moreover, the thymine allylic radical intermediate needs to be quenched by abstracting an H-atom from C74. The two species involved need to be correctly positioned for an efficient H-atom transfer to occur; the increased mobility in $SPL_{(Ca)}$ active site, however, will certainly make transfer more difficult. Collectively, these aspects are likely responsible for the 10-fold slower SP TpT repair by $SPL_{(Ca)}$ than by $SPL_{(Bs)}$. The different yield of runaway product $TpTSO_2^-$ may also be explained in a similar way. The more flexible active site in $SPL_{(Ca)}$ results in weaker binding interactions, not only with the SP TpT substrate, but also with reaction intermediates such as the thymine allylic radical, which is then quenched by the external sodium dithionite leading to $TpTSO_2^-$. Therefore,

the 4-fold higher yield of $TpTSO_2^-$ in the $SPL_{(Ca)}$ reaction is also consistent with the more flexible active site in this protein.

The rationale also explains the different apparent ($^D V$) and competitive ($^D V/K$) KIEs observed for these two enzymes. As explained previously, the H-abstraction from the methyl group of 5'-dA by the tyrosine radical ($Y99_{(Bs)}$) likely possesses the highest energy barrier (16) among all steps; this step is considered to be the rate-determining step at the steady state (36). Correspondingly, all prior steps belong to the so-called “rate-determining zone (RDZ)” and contribute to the overall reaction rate (Figure 13A) (37). The deuterium isotope sensitive step (i.e., the H(D) abstraction by 5'-dA• generated by the SAM reductive cleavage) results in the so-called intrinsic kinetic isotope effect. As this step is located in the RDZ, the intrinsic KIE is responsible for the slowdown of the overall enzyme reaction when d_4-SP is used as the substrate, leading to the ($^D V$) and ($^D V/K$) KIEs observed here.

To understand further the different ($^D V$) and ($^D V/K$) KIEs between $SPL_{(Bs)}$ and $SPL_{(Ca)}$, we simplified the enzyme reaction by using the method of Northrop (Figure 13B) (35). Here, k_a is an apparent first-order rate constant for the breakdown of the enzyme-substrate complexes ES and ES' to free enzyme and substrate; k_b is an apparent first-order rate constant for the conversion of the first enzyme complex following substrate binding to the first enzyme complex immediately following the first irreversible step of the reaction; and k_c is the apparent first-order rate constant for the conversion of the enzyme complex immediately following the first irreversible step to free enzyme. Because the more flexible $SPL_{(Ca)}$ active site is expected to lead to weaker enzyme-substrate interactions and a less stable Michaelis complex, it is reasonable to assume that $k_{a(Ca)}$ is much larger than $k_{a(Bs)}$ owing to the much faster substrate dissociation, $k_{b(Ca)}$ is smaller than $k_{b(Bs)}$ as rationalized above, and $k_{c(Ca)}$ is probably larger than $k_{c(Bs)}$, again owing to the enhanced active-site mobility resulting in weaker binding interactions.

Our previous studies determined a primary apparent KIE of 2.9 ± 0.3 for $SPL_{(Bs)}$ (13, 16), which is smaller than the apparent KIEs of 6.1 ± 0.7 for TpT and 5.8 ± 1.0 for $TpTSO_2^-$ mediated by $SPL_{(Ca)}$. To explain the different ($^D V$) KIEs, we turn to the equation below as originally described by Northrop (35):

$$\frac{V_H}{V_D} = \frac{k_{bH}/k_{bD} + (k_b/k_c)_H}{(k_b/k_c)_H + 1}$$

As shown in Figure 13A, we made a reasonable assumption that comparing with the $SPL_{(Bs)}$ reaction, $SPL_{(Ca)}$ only destabilizes the Michaelis complex resulting in smaller k_b. Although both $k_{bH(Ca)}$ and $k_{bD(Ca)}$ are smaller than $k_{bH(Bs)}$ and $k_{bD(Bs)}$, respectively, the ratio between them is unlikely to vary considerably given that k_b reflects all steps between ES and EP′ including the isotope-sensitive step. In contrast, the $(k_b/k_c)_H$ will be smaller in $SPL_{(Ca)}$ as k_{bH} is smaller whereas k_{cH} is likely larger. As a consequence, the ($^D V$) KIE in $SPL_{(Ca)}$, compared to that of $SPL_{(Bs)}$, is projected to be closer to the original ratio of k_{bH}/k_{bD} (35), resulting in a bigger ($^D V$) KIE as observed in this report. Moreover, after the formation of the thymine allylic radical (T-CH_2•, Figure 13A), although its quenching by C74 is

presumably fast, the quenching step is followed by the heavily uphill (thus slow) H-abstraction step from the methyl group of 5'-dA mediated by the tyrosyl radical. In contrast, the radical quenching by sodium dithionite leading to $TpTSO_2^-$ may be slow; however, the product does not need to react further with 5'-dA. Therefore, collectively these two processes may generate not-so-different k_{bH} and k_{bD}, offering an explanation for the similar apparent ($^D V$) KIEs observed for the formation of TpT and $TpTSO_2^-$ by $SPL_{(Ca)}$.

Similarly, the abnormally large competitive ($^D V/K$) KIEs observed in the $SPL_{(Ca)}$ reaction can also be explained. In most cases, k_a does not show an isotope effect. Consequently, the ($^D V/K$) KIE is represented by the equation below (35):

$$\frac{(V/K)_H}{(V/K)_D} = \frac{k_{bH}/k_{bD} + (k_b/k_a)_H}{(k_b/k_a)_H + 1}$$

As shown previously, $SPL_{(Bs)}$ exhibits a competitive KIE of 3.4 ± 0.3 (16), which is much smaller than the 17.0 ± 2.0 for TpT and 21.0 ± 2.0 for $TpTSO_2^-$ observed here. As described above, we do not expect a drastically different k_{bH}/k_{bD} for $SPL_{(Ca)}$ and $SPL_{(Bs)}$. However, $k_{a(Ca)}$ is likely much larger than $k_{a(Bs)}$. Given that $k_{b(Ca)}$ is smaller than $k_{b(Bs)}$, $(k_b/k_a)_{H(Ca)}$ can be very small and, thus, negligible. Consequently, the ($^D V/K$) KIE can be very close to the k_{bH}/k_{bD} in $SPL_{(Ca)}$, explaining the abnormally large ($^D V/K$) KIEs for both TpT and $TpTSO_2^-$ formation observed here.

Taken together, using the smallest substrate dinucleotide SP TpT, which is indicated to have a weak binding affinity toward SPL, we were able to obtain experimental evidence supporting the assumption that $SPL_{(Ca)}$ possesses a more flexible active site than its *B. subtilis* counterpart. This flexibility, then, facilitates the projected protein conformational changes to enable radical transfer from the conserved cysteine to downstream tyrosine. Therefore, $SPL_{(Ca)}$ represents a novel example in which an enzyme uses relatively large protein conformational changes to facilitate radical transfer. Even though the studies of class I ribonucleotide reductase suggest that protein conformational changes are used to gate the radical-transfer direction (38), to our knowledge the large conformational changes implied in $SPL_{(Ca)}$ resulting from the swing of protein loops after product release and the collapse of the enzyme binding pocket are unprecedented for radical enzymes. Although SPL enzymes from *Bacillus* and *Clostridium* strains may utilize the same radical-transfer process, they appear to undergo different levels of protein motion to achieve efficient catalysis.

Supplementary Material

Refer to Web version on PubMed Central for supplementary material.

Acknowledgments

This work was supported in part by National Institutes of Health Grant ES017177 and the National Science Foundation CHE1506598 (to L.L.). The HDX studies were supported by NIH, NIGMS Grant P41GM103422 (to M.L.G.). The NMR and MS facilities at IUPUI were supported by National Science Foundation MRI grants CHE-0619254 and DBI-0821661, respectively.

REFERENCES

1. Desnous CL, Guillaume D, Clivio P. Spore photoproduct: A key to bacterial eternal life. Chem. Rev. 2010; 110:1213–1232. [PubMed: 19891426]
2. Nicholson W, Schuerger A, Setlow P. The solar UV environment and bacterial spore UV resistance: Considerations for earth-to-mars transport by natural processes and human spaceflight. Mutat. Res. Fund. Mol. Mech. Mut. 2005; 571:249–264.
3. Nicholson WL, Munakata N, Horneck G, Melosh HJ, Setlow P. Resistance of *Bacillus* endospores to extreme terrestrial and extraterrestrial environments. Microbiol. Mol. Biol. Rev. 2000; 64:548–572. [PubMed: 10974126]
4. Setlow P, Li L. Photochemistry and photobiology of the spore photoproduct: A 50-year journey. Photochem. Photobiol. 2015; 91:1263–1290. [PubMed: 26265564]
5. Yang L, Li L. Spore photoproduct lyase: The known, the controversial, and the unknown. J. Biol. Chem. 2015; 290:4003–4009. [PubMed: 25477522]
6. Setlow B, Setlow P. Decreased UV light resistance of spores of *Bacillus subtilis* strains deficient in pyrimidine dimer repair and small, acid-soluble spore proteins. Appl. Environ. Microbiol. 1988; 54:1275–1276. [PubMed: 3133982]
7. Setlow P. Mechanisms for the prevention of damage to DNA in spores of *Bacillus* species. Annu. Rev. Microbiol. 1995; 49:29–54. [PubMed: 8561462]
8. Sofia HJ, Chen G, Hetzler BG, Reyes-Spindola JF, Miller NE. Radical SAM, a novel protein superfamily linking unresolved steps in familiar biosynthetic pathways with radical mechanisms: Functional characterization using new analysis and information visualization methods. Nucleic Acids Res. 2001; 29:1097–1106. [PubMed: 11222759]
9. Broderick JB, Duffus BR, Duschene KS, Shepard EM. Radical *S*-adenosylmethionine enzymes. Chem. Rev. 2014; 114:4229–4317. [PubMed: 24476342]
10. Frey P, Magnusson O. S-adenosylmethionine: A wolf in sheep's clothing, or a rich man's adenosylcobalamin? Chem. Rev. 2003; 103:2129–2148. [PubMed: 12797826]
11. Yang L, Li L. The enzyme-mediated direct reversal of a dithymine photoproduct in germinating endospores. Int. J. Mol. Sci. 2013; 14:13137–13153. [PubMed: 23799365]
12. Mehl RA, Begley TP. Mechanistic studies on the repair of a novel DNA photolesion: The spore photoproduct. Org. Lett. 1999; 1:1065–1066. [PubMed: 10825958]
13. Yang L, Lin G, Liu D, Dria KJ, Telser J, Li L. Probing the reaction mechanism of spore photoproduct lyase (SPL) via diastereoselectively labeled dinucleotide SP TpT substrates. J. Am. Chem. Soc. 2011; 133:10434–10447. [PubMed: 21671623]
14. Yang L, Lin G, Nelson RS, Jian Y, Telser J, Li L. Mechanistic studies of the spore photoproduct lyase via a single cysteine mutation. Biochemistry. 2012; 51:7173–7188. [PubMed: 22906093]
15. Fajardo-Cavazos P, Rebeil R, Nicholson W. Essential cysteine residues in *Bacillus subtilis* spore photoproduct lyase identified by alanine scanning mutagenesis. Curr. Microbiol. 2005; 51:331–335. [PubMed: 16163454]
16. Yang L, Nelson RS, Benjdia A, Lin G, Telser J, Stoll S, Schlichting I, Li L. A radical transfer pathway in spore photoproduct lyase. Biochemistry. 2013; 52:3041–3050. [PubMed: 23607538]
17. Benjdia A, Heil K, Barends TRM, Carell T, Schlichting I. Structural insights into recognition and repair of UV-DNA damage by spore photoproduct lyase, a radical SAM enzyme. Nucleic Acids Res. 2012; 40:9308–9318. [PubMed: 22761404]
18. Benjdia A, Heil K, Winkler A, Carell T, Schlichting I. Rescuing DNA repair activity by rewiring the H-atom transfer pathway in the radical SAM enzyme, spore photoproduct lyase. Chem. Commun. 2014; 50:14201–14204.
19. Yang C-G, Yi C, Duguid EM, Sullivan CT, Jian X, Rice PA, He C. Crystal structures of DNA/RNA repair enzymes AlkB and ABH2 bound to dsDNA. Nature. 2008; 452:961–965. [PubMed: 18432238]
20. Roberts RJ, Cheng X. Base flipping. Annu. Rev. Biochem. 1998; 67:181–198. [PubMed: 9759487]
21. Butenandt J, Burgdorf LT, Carell T. "Base flipping": Photodamaged DNA-RNA duplexes are poor substrates for photoreactivating DNA-repair enzymes. Angew. Chem. Int. Ed. 1999; 38:708–711.

22. Liu Z, Tan C, Guo X, Kao Y-T, Li J, Wang L, Sancar A, Zhong D. Dynamics and mechanism of cyclobutane pyrimidine dimer repair by DNA photolyase. Proc. Natl. Acad. Sci. 2011; 108:14831–14836. [PubMed: 21804035]
23. Maul M, Barends TM, Glas AF, Cryle M, Domratcheva T, Schneider S, Schlichting I, Carell T. Crystal structure and mechanism of a DNA (6–4) photolyase. Angew. Chem. Int. Ed. 2008; 47:10076–10080.
24. Christine KS, Macfarlane AW, Yang K, Stanley RJ. Cyclobutylpyrimidine dimer base flipping by DNA photolyase. J. Biol. Chem. 2002; 277:38339–38344. [PubMed: 12169694]
25. Lin G, Li L. Elucidation of spore-photoproduct formation by isotope labeling. Angew. Chem. Int. Ed. 2010; 49:9926–9929.
26. Cicchillo RM, Iwig DF, Jones AD, Nesbitt NM, Baleanu-Gogonea C, Souder MG, Tu L, Booker SJ. Lipoyl synthase requires two equivalents of *S*-adenosyl-L-methionine to synthesize one equivalent of lipoic acid. Biochemistry. 2004; 43:6378–6386. [PubMed: 15157071]
27. Chatterjee A, Li Y, Zhang Y, Grove TL, Lee M, Krebs C, Booker SJ, Begley TP, Ealick SE. Reconstitution of ThiC in thiamine pyrimidine biosynthesis expands the radical SAM superfamily. Nat. Chem. Biol. 2008; 4:758–765. [PubMed: 18953358]
28. Pedraza-Reyes M, Gutierrez-Corona F, Nicholson WL. Spore photoproduct lyase operon (*splAB*) regulation during *Bacillus subtilis* sporulation: Modulation of *splB-lacZ* fusion expression by P1 promoter mutations and by an in-frame deletion of *splA*. Curr. Microbiol. 1997; 34:133–137. [PubMed: 9009064]
29. Yan Y, Grant GA, Gross ML. Hydrogen-deuterium exchange mass spectrometry reveals unique conformational and chemical transformations occurring upon [4Fe-4S] cluster binding in the type 2 L-serine dehydratase from *Legionella pneumophila*. Biochemistry. 2015; 54:5322–5328. [PubMed: 26266572]
30. Pascal BD, Willis S, Lauer JL, Landgraf RR, West GM, Marciano D, Novick S, Goswami D, Chalmers MJ, Griffin PR. HDX workbench: Software for the analysis of H/D exchange MS data. J. Am. Soc. Mass. Spectrom. 2012; 23:1512–1521. [PubMed: 22692830]
31. Nakamaru-Ogiso E, Yano T, Ohnishi T, Yagi T. Characterization of the iron-sulfur cluster coordinated by a cysteine cluster motif (CxxCxxxCx 27C) in the Nqo3 subunit in the proton-translocating NADH-quinone oxidoreductase (NDH-1) of *Thermus thermophilus* HB-8. J. Biol. Chem. 2002; 277:1680–1688. [PubMed: 11704668]
32. Chandor-Proust A, Berteau O, Douki T, Gasparutto D, Ollagnier-De-Choudens S, Fontecave M, Atta M. DNA repair and free radicals, new insights into the mechanism of spore photoproduct lyase revealed by single amino acid substitution. J. Biol. Chem. 2008; 283:36361–36368. [PubMed: 18957420]
33. Lin G, Li L. Oxidation and reduction of the 5-(2′-deoxyuridinyl)methyl radical. Angew. Chem. Int. Ed. 2013; 52:5594–5598.
34. Landgraf BJ, Mccarthy EL, Booker SJ. Radical *S*-adenosylmethionine enzymes in human health and disease. Annu. Rev. Biochem. 2016; 85:485–514. [PubMed: 27145839]
35. Northrop DB. Steady-state analysis of kinetic isotope effects in enzymic reactions. Biochemistry. 1975; 14:2644–2651. [PubMed: 1148173]
36. Yagisawa S. Two types of rate-determining step in chemical and biochemical processes. Biochem. J. 1989; 263:985–988. [PubMed: 2597141]
37. Yagisawa S. Enzyme kinetics based on free-energy profiles. Biochem. J. 1995; 308(Pt 1):305–311. [PubMed: 7755578]
38. Minnihan EC, Nocera DG, Stubbe J. Reversible, long-range radical transfer in *E. coli* class Ia ribonucleotide reductase. Acc. Chem. Res. 2013; 46:2524–2535. [PubMed: 23730940]

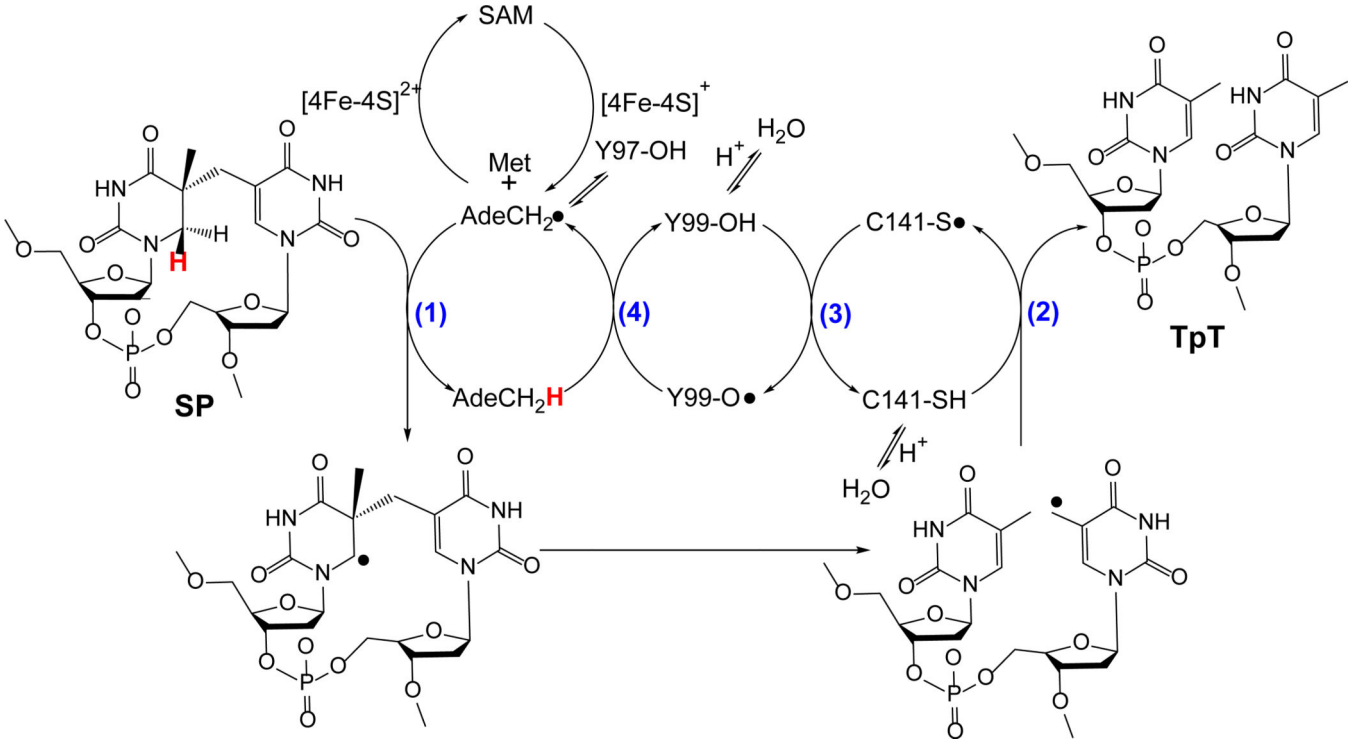

Figure 1.

The currently hypothesized reaction mechanism for SPL (amino acid residues are numbered according to the protein sequence in *Bacillus subtilis* (*Bs*) SPL). This mechanism implies that SPL uses a minimum of four H-atom transfer steps (numbers in blue) in each catalytic cycle. Y97 is hypothesized to facilitate the H-abstraction from the methyl group of 5'-dA by stabilizing the resulting 5'-dA• via radical delocalization.

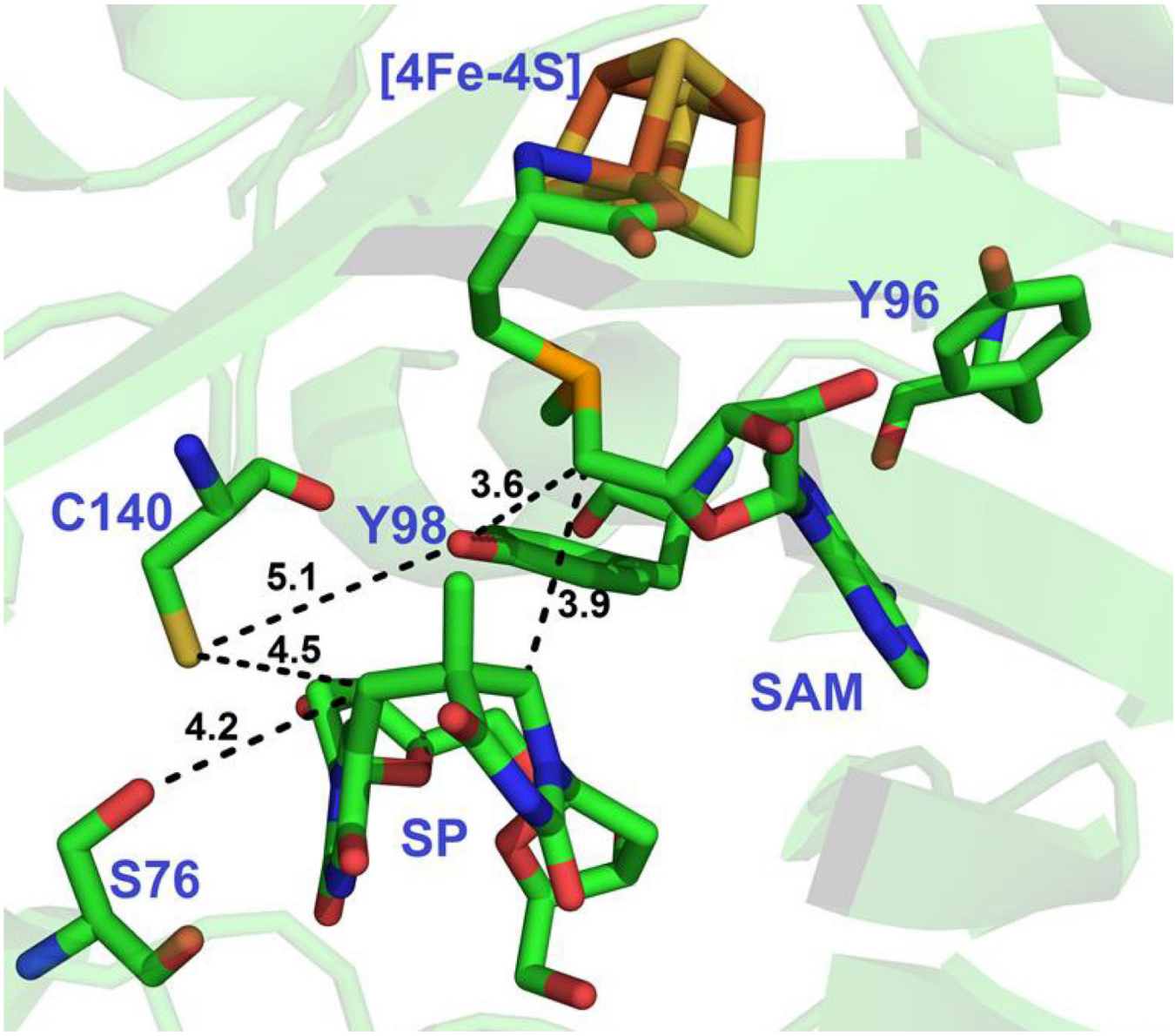

Figure 2.

Active site structure of *Geobacillus thermodenitrificans* (*Gt)* SPL in complex with SP and SAM. The $C140_{(Gt)}$, $Y96_{(Gt)}$ and $Y98_{(Gt)}$ residues correspond to the $C141_{(Bs)}$, $Y97_{(Bs)}$ and $Y99_{(Bs)}$ residues in $SPL_{(Bs)}$ respectively. The distances between selected protein residues, SP, and SAM are given next to the corresponding dashed lines (PDB code 4FHD).

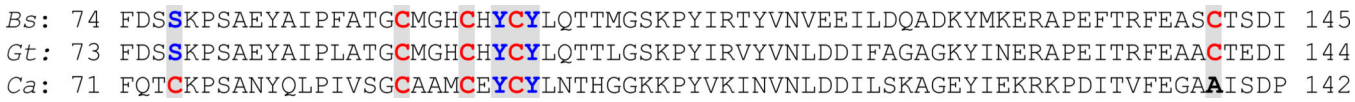

Figure 3.

The partial sequences of SPL enzymes from *B. subtilis* (*Bs*), *G. thermodenitrificans* (*Gt*) and *C. acetobutylicum* (*Ca*), showing the key amino acids involved in the radical transfer process.

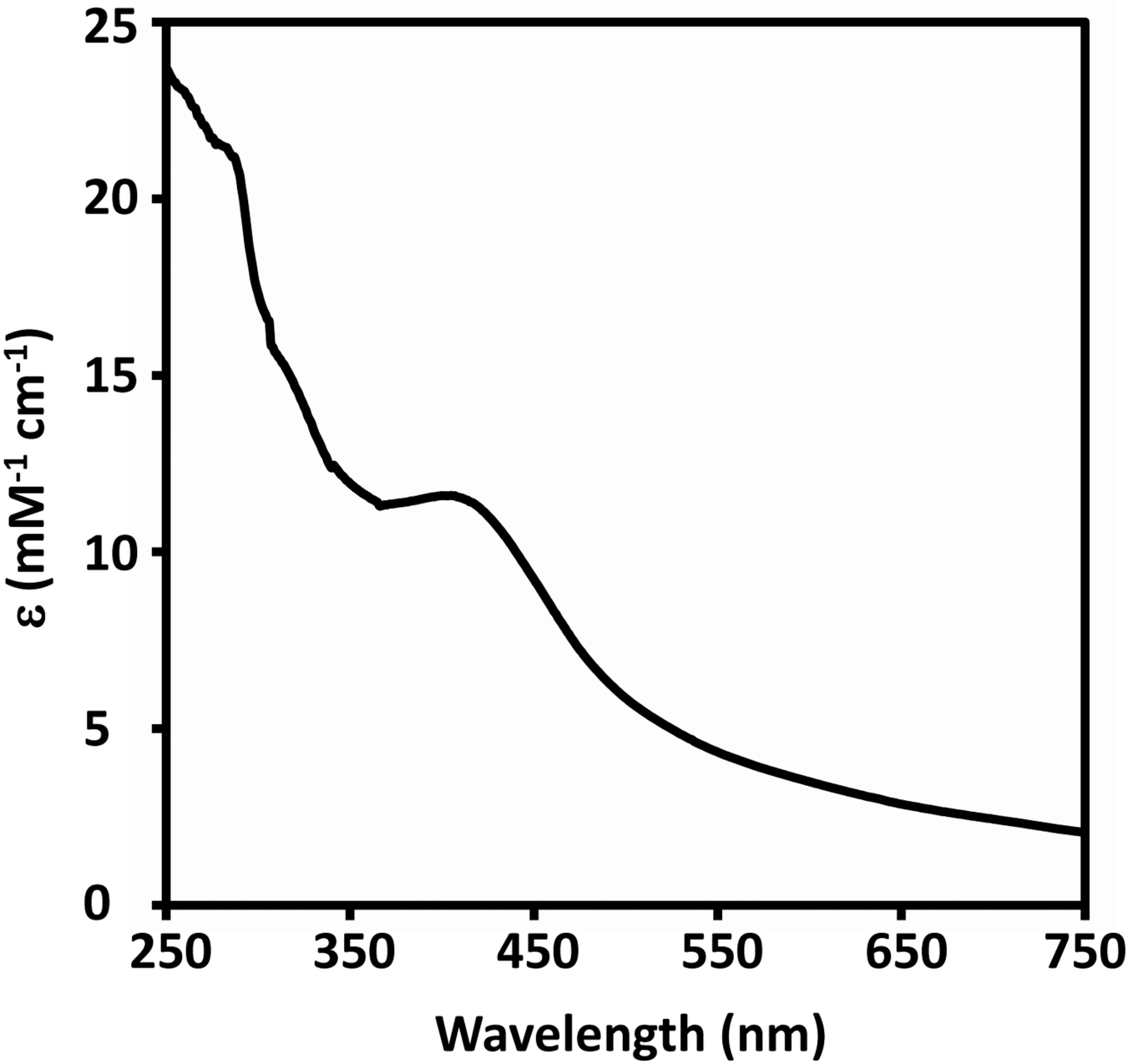

Figure 4.

UV-visible spectrum of the as-isolated $SPL_{(Ca)}$. The spectrum is featured by a shoulder-like absorption peak at 408 nm, which is the characteristic absorption band for the $[4Fe\text{-}4S]^{2+}$ cluster.

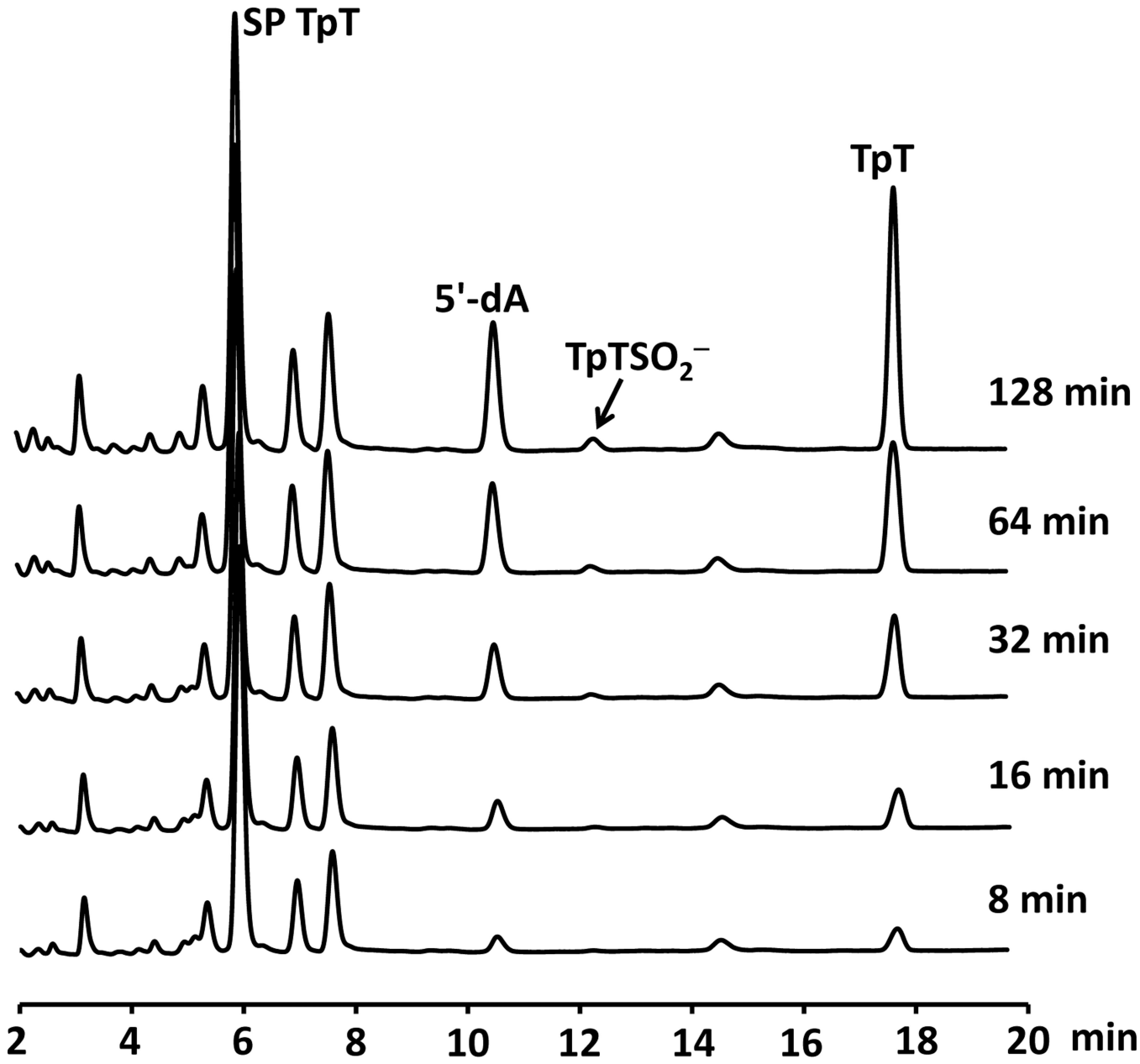

Figure 5.

HPLC chromatograms describing the SP TpT repair mediated by the wildtype $SPL_{(Bs)}$ with 30 μM enzyme, 150 μM SAM and 1 mM dithionite. The TpT formation rate was found at ~ 0.38 min^{-1}. Formation of TpT-SO_2^- was obvious after a 0.5-hr enzyme reaction; the formed TpT-SO_2^- accounted for ~ 5% of the overall SP repaired.

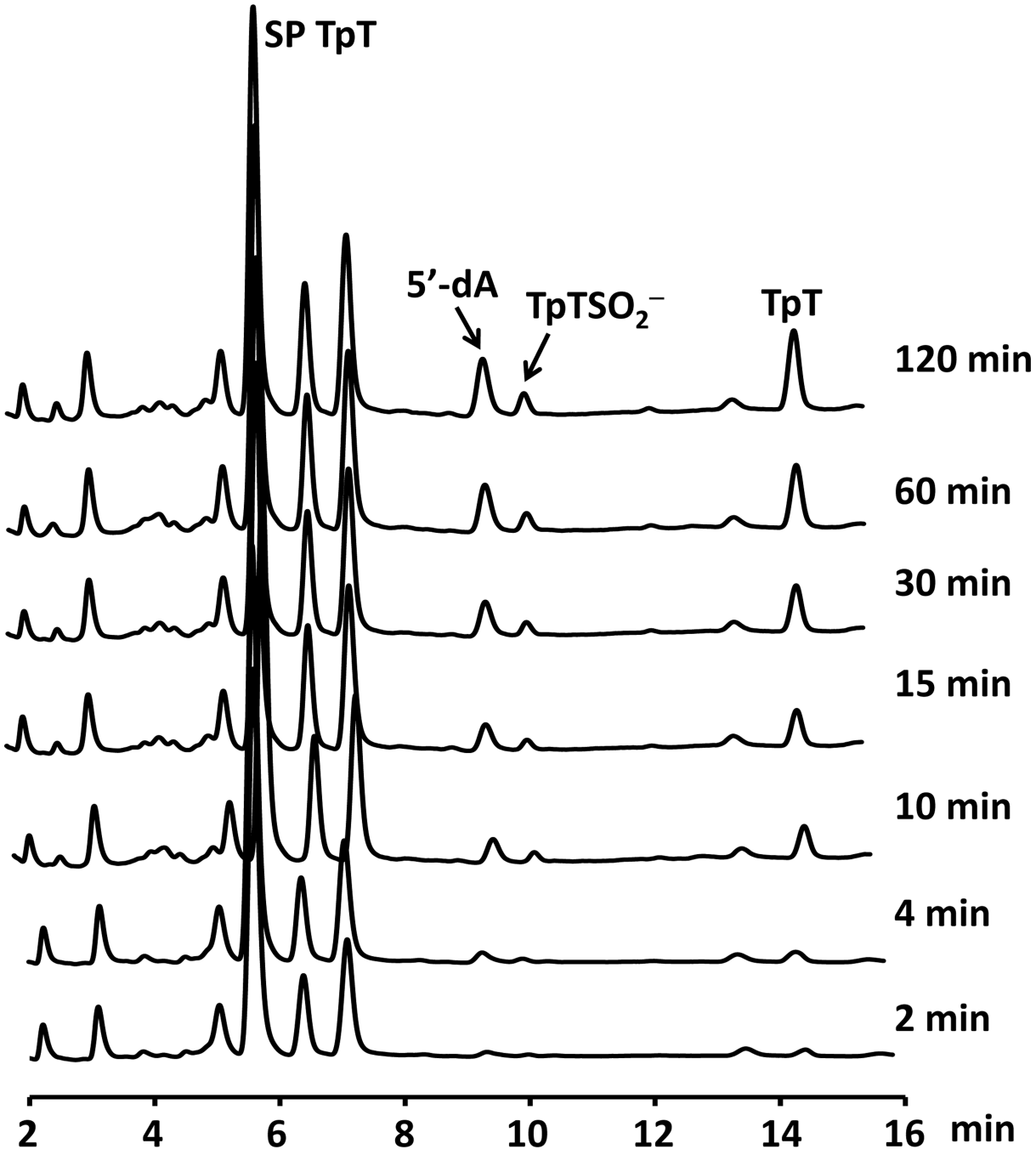

Figure 6.

HPLC chromatogram of the SP TpT repair mediated by the wildtype $SPL_{(Ca)}$ enzyme with 30 μM enzyme, 150 μM SAM and 1 mM dithionite. The TpT formation rate was determined at ~ 0.04 min^{-1}. Formation of TpT-SO_2^- was obvious from the very beginning of the SP repair reaction; the formed TpT-SO_2^- accounted for ~ 20% of overall SP repaired.

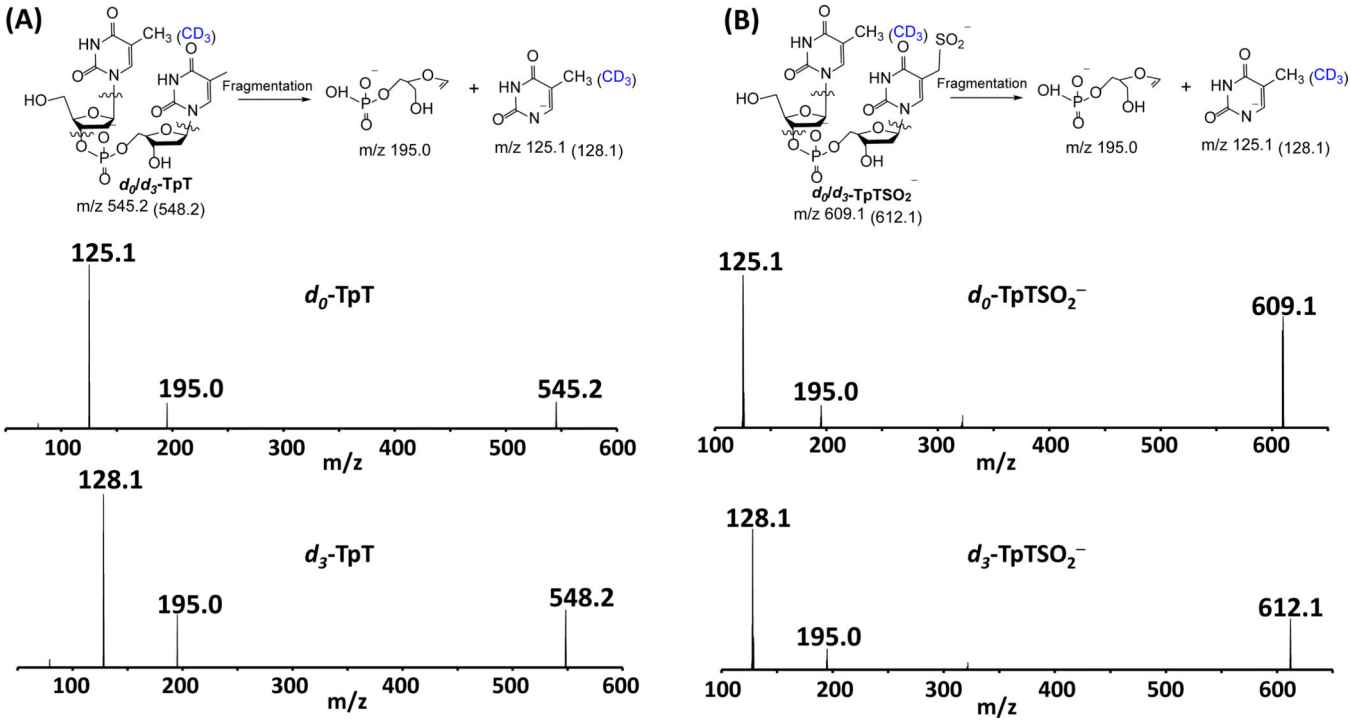

Figure 7.

(A) The chemical structures of the repair products d_0-/d_3-TpT and the two major fragments observed in ESI-MS analysis in the negative-ion mode. The fragment signals corresponding to ions of *m/z* 125.1 and 128.1 from the 5'-thymine daughter ion were used to quantify the ratio of the formed d_0- and d_3-TpT via MS/MS. (B) The chemical structures of d_0-/d_3-$TpTSO_2^-$ and the two major fragments observed in ESI-MS analysis under the negative ion mode. Again, fragment signals of *m/z* 125.1 and 128.1 corresponding to the 5'-thymine daughter ion were used to quantify the ratio of the formed d_0- and d_3-$TpTSO_2^-$ via MS/MS.

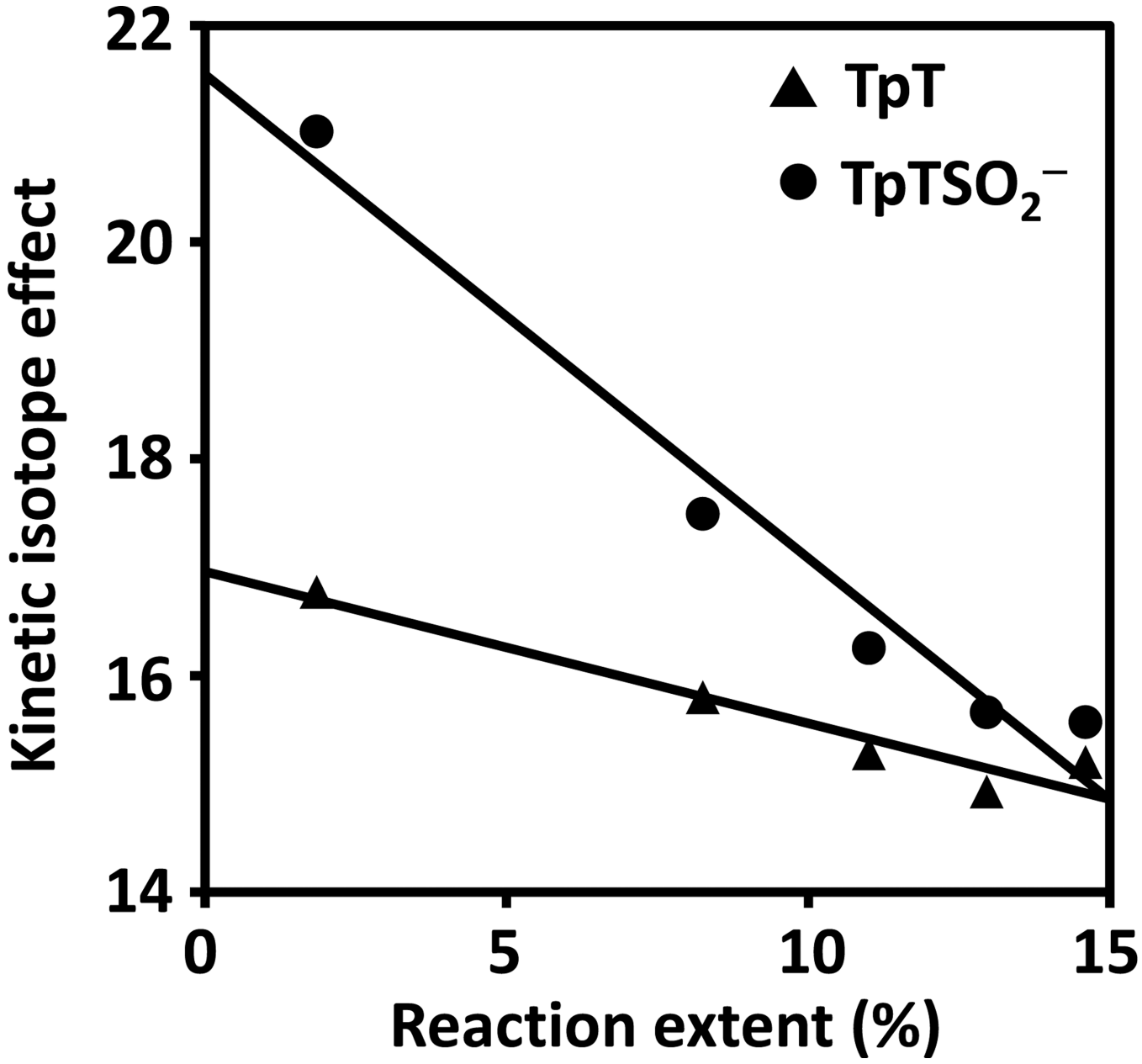

Figure 8.

Determination of the competitive ($^{D}V/K$) isotope effect by extrapolation of the measured KIEs to zero extent of reaction. The competitive KIE was determined to be 17.0 ± 2.0 for TpT formation (▲) or 21.0 ± 2.0 for $TpTSO_2^-$ (●) formation.

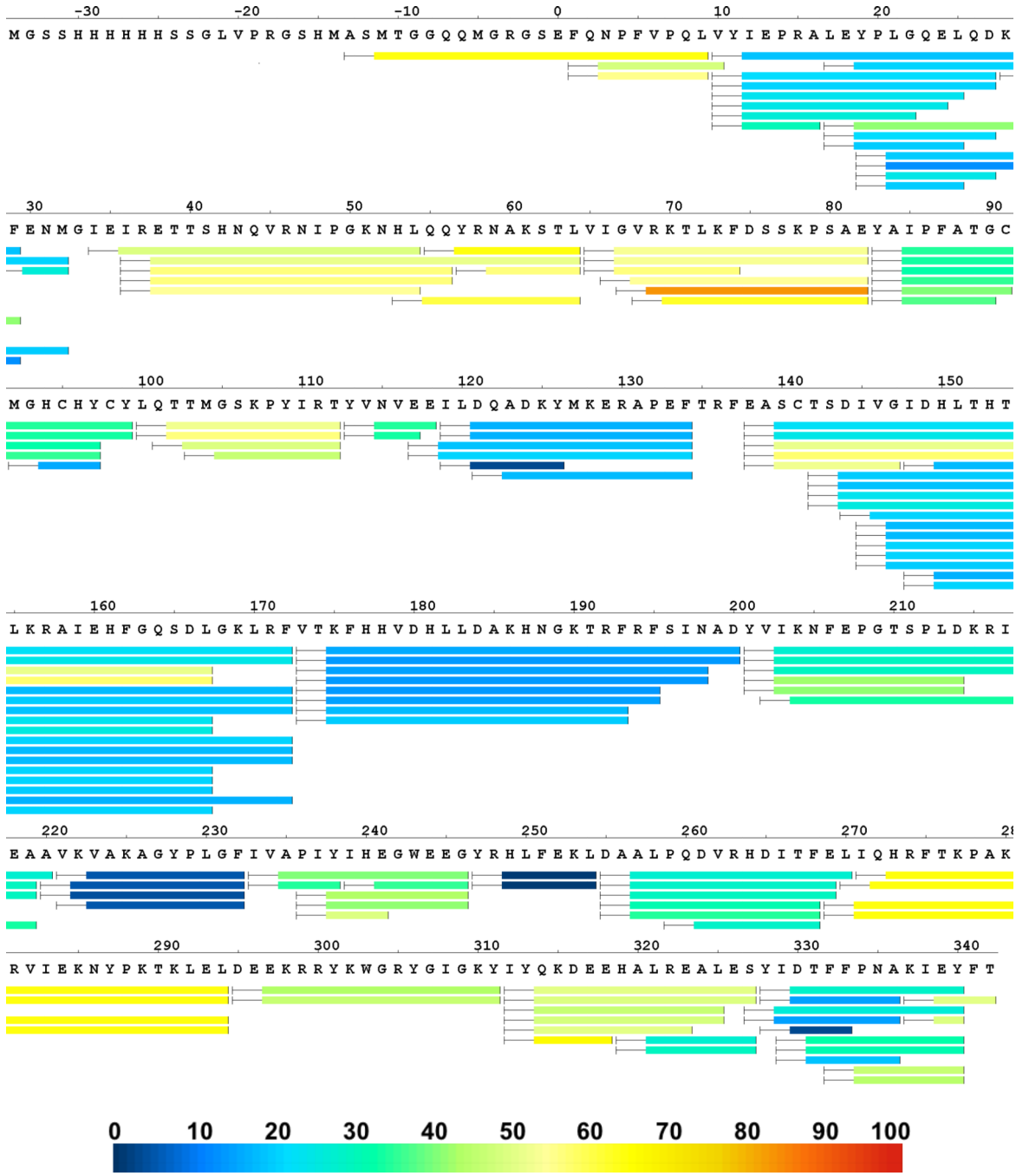

Figure 9.

Sequence coverage map of peptic digestion of $SPL_{(Bs)}$. A total of 128 peptides with a sequence coverage of 99% were identified. Each bar indicates a peptide identified by mass spectrometry. The colored bars represent the average deuterium uptake percentage (D%) for the duplicate analysis of seven exchange time points (the warmer the color the higher the deuterium uptake). Please note that the actual protein sequence starts from the second amino acid residue as the first residue (i.e., the methionine residue) was deleted during the construction of the expression vector.

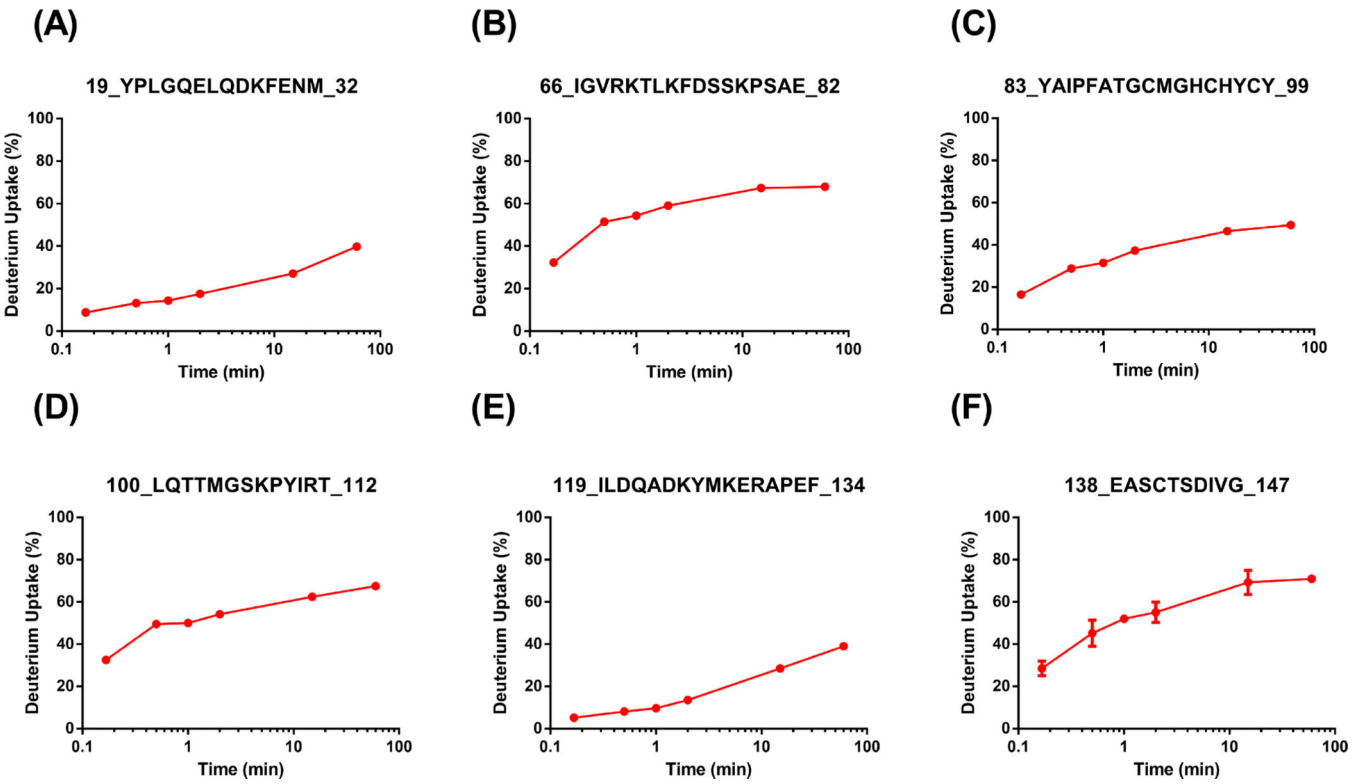

Figure 10.

Peptide-level HDX kinetics of a peptide from the binding site in $SPL_{(Bs)}$ (C). Also shown are the peptides neighboring the binding sites in the protein (A, B and D-F).

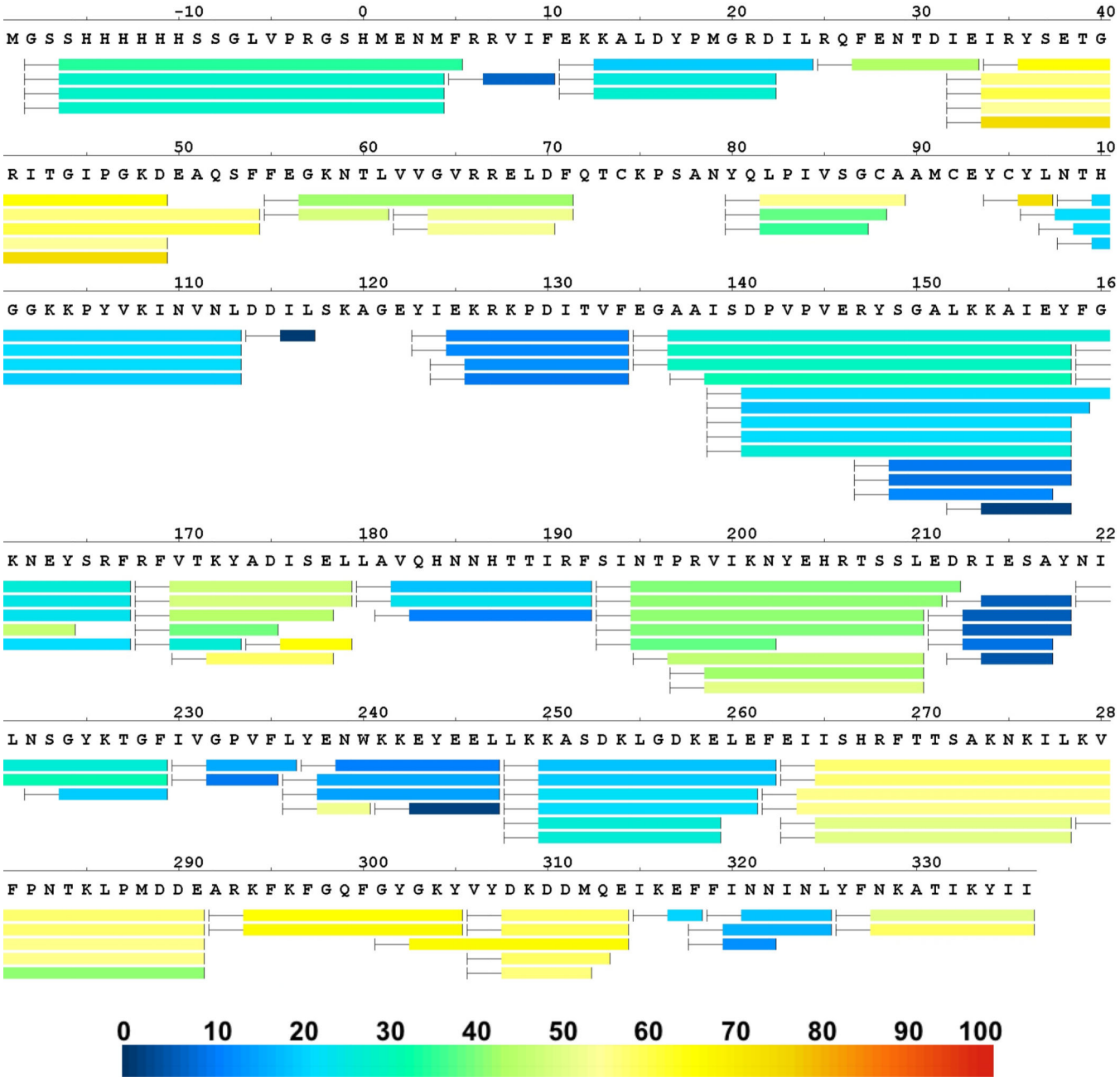

Figure 11.

Sequence coverage map of peptic digestion of $SPL_{(Ca)}$. Each bar indicates a peptide identified by mass spectrometry. A total of 106 peptides with a sequence coverage of 95% were identified. The colored bars represent the average deuterium uptake percentages (D%) for the duplicate analysis of seven exchange time points (the warmer the color the higher the deuterium uptake). Please note that the actual protein sequence starts from the second amino acid residue as the first residue (i.e., the methionine residue) was deleted during the construction of the expression vector.

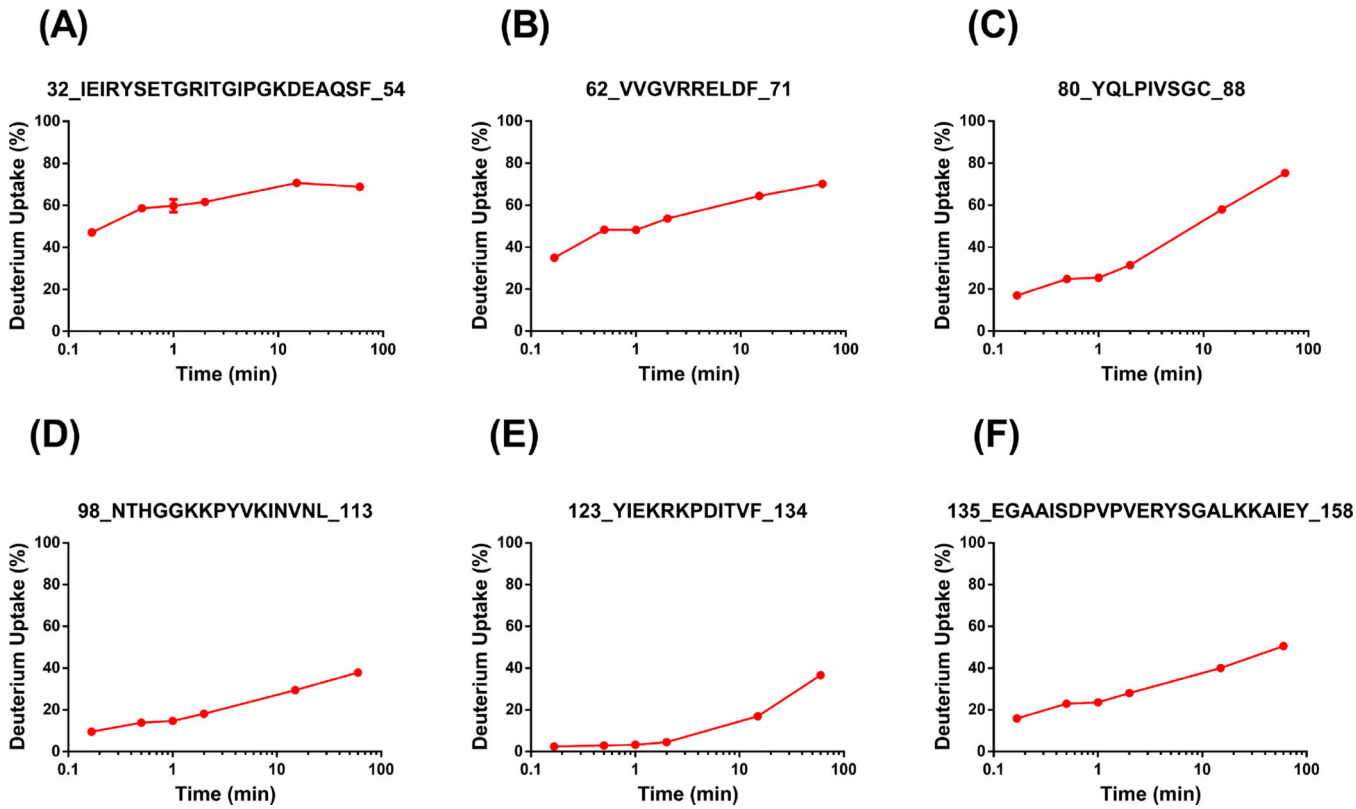

Figure 12.

Peptide-level HDX kinetics representing the binding site in $SPL_{(Ca)}$ (12C) and the neighboring regions as represented by corresponding peptides (12 A, B and D-F).

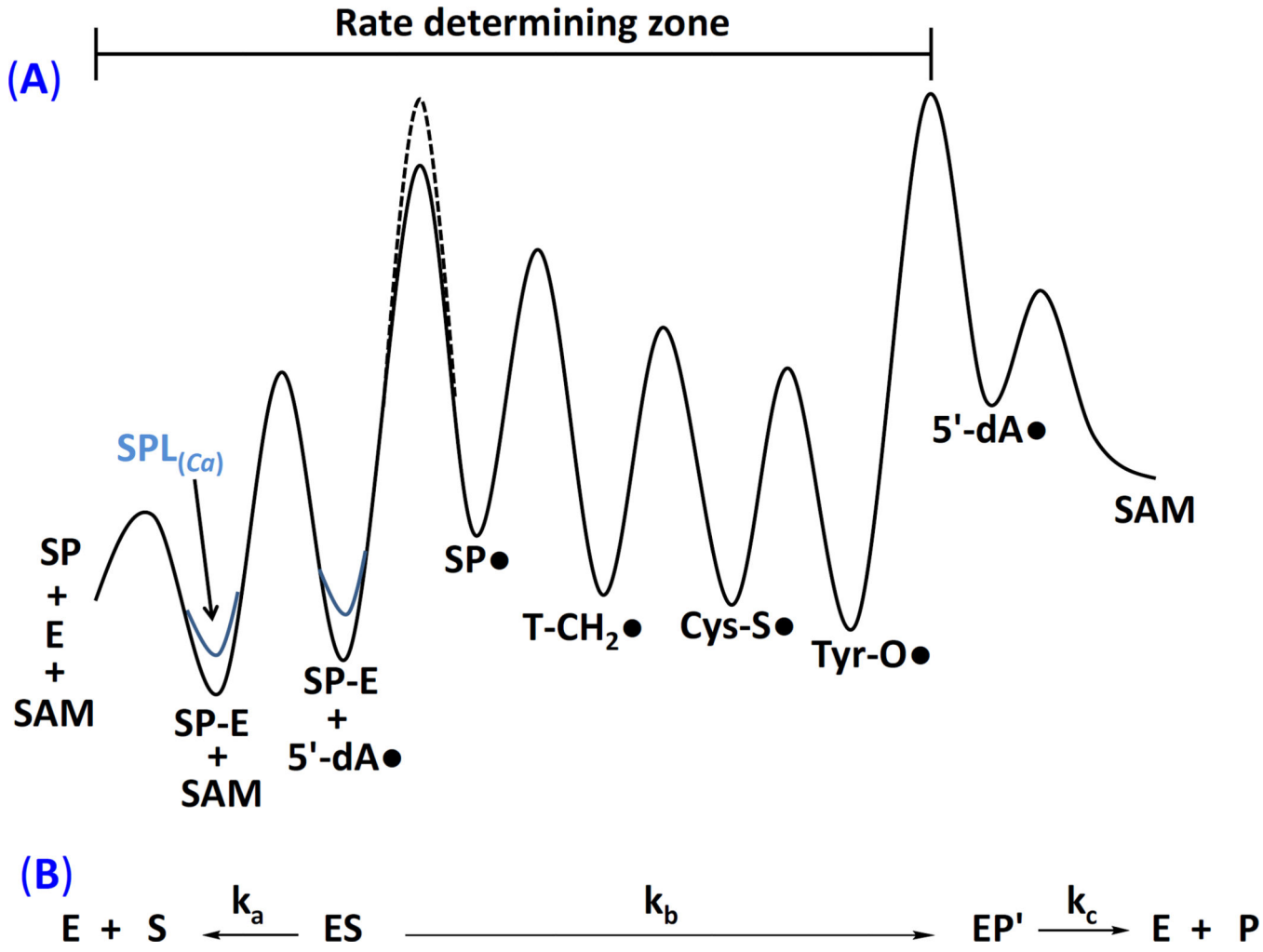

Figure 13.

(A) Sketch of the free energy profile for the SPL catalyzed SP repair reaction. The blackline represents the SP repair process catalyzed by $SPL_{(Bs)}$. We simplified the drawing by making a reasonable hypothesis that all other steps for the $SPL_{(Ca)}$ reaction are similar to those in $SPL_{(Bs)}$ except for the binding step with dinucleotide SP TpT, where the more flexible $SPL_{(Ca)}$ active site results in a weaker SP binding and a less stable Michaelis complex (SP-E). The increased energy barrier when d_4-SP is used as the substrate is indicated by dashed lines. (B) Simplification of the enzyme reaction using the definition adopted by Northrop (35).